

Characterizing Binary Black Hole Subpopulations in GWTC-4 with Binned Gaussian Processes: On the Origins of the $35M_{\odot}$ Peak.

OMKAR SRIDHAR^{1,2}, ANARYA RAY^{2,3} AND VICKY KALOGERA^{1,2,3}

¹*Department of Physics and Astronomy, Northwestern University, 2145 Sheridan Road, Evanston, IL 60208, USA*

²*Center for Interdisciplinary Exploration and Research in Astrophysics (CIERA), Northwestern University, 1800 Sherman Ave, Evanston, IL 60201, USA*

³*NSF-Simons AI Institute for the Sky (SkAI), 172 E. Chestnut Street, Chicago, IL 60611, USA*

(Dated: December 1, 2025)

ABSTRACT

Understanding the astrophysical origins of binary black holes requires accurate and flexible modeling of multi-dimensional population properties. In this paper, using a data-driven framework based on binned Gaussian processes, we characterize the joint distribution of BBH primary masses, mass ratios, and effective inspiral spins. We identify three distinct subpopulations in the GWTC-4 sample of observations and investigate their astrophysical origins. We find that only one of the three subpopulations exhibits the $35M_{\odot}$ peak, which is characterized by a strong preference for equal mass systems and isotropic spin orientations. Our inferred distributions are consistent with a predominantly dynamical origin of this feature. By comparing with theoretical simulations, we further show that the subpopulation that exhibits the $35M_{\odot}$ peak can exclusively comprise dynamically assembled systems in globular clusters, specifically if black hole birth spins are in the range $(0.1 - 0.2)$, whereas the other two subpopulations require substantial contributions from alternative formation channels. We constrain the *lower bound* on the merger rate of BBHs in globular clusters to be $0.69^{+0.23}_{-0.33} \text{Gpc}^{-3} \text{yr}^{-1}$, which is consistent with theoretical predictions. We conclude that dynamical formation in globular clusters remains a strong candidate for the origin of this excess near $30 - 40M_{\odot}$ and that more data and targeted parametric models are necessary to rigorously establish this interpretation.

1. INTRODUCTION

The fourth observing run of the LIGO-Virgo-KAGRA detector network (LVK; Abac et al. 2025a; Aasi et al. 2015; Acernese et al. 2014; Akutsu et al. 2021) concluded its first set this year, and 153 confidently identified binary black hole (BBH) signals were released as part of the fourth gravitational wave transient catalog (GWTC-4; Abac et al. 2025b). With a growing number of gravitational wave (GW) observations by the LVK, studying the population properties of BBH parameters and the correlations between them provides a unique opportunity to probe the astrophysical phenomena that led to the formation of these GW progenitors. Currently proposed mechanisms for BBH formation include isolated binary evolution in galactic fields (Porte-

gies Zwart & Yungelson 1998; Belczynski et al. 2001; Stevenson et al. 2017); dynamical formation in dense environments (Kulkarni et al. 1993; Sigurdsson & Hernquist 1993; Portegies Zwart & McMillan 2000; Ziosi et al. 2014); and hierarchical mergers in stellar clusters (Fishbach et al. 2017; Gerosa & Berti 2017; Rodriguez et al. 2019; Doctor et al. 2020; Kimball et al. 2021) and disks of active galactic nuclei (Stone et al. 2017; Bartos et al. 2017; McKernan et al. 2020). The unconstrained physical phenomena that underlie these evolutionary pathways can, in principle, be elucidated by identifying their imprints as specific population features in the observed sample of BBHs.

As the detection sample continues to grow, two key features in the BBH mass spectrum have emerged as robust characteristics of the underlying population. A sharp peak near $10M_{\odot}$ and an over-abundance of systems near $35M_{\odot}$ have been reported in GWTC-4 using a large number of both strongly parametrized and flexible population models, all of which broadly agree on their

omkarnm1401@gmail.com

anarya.ray@northwestern.edu

nature and existence (Abac et al. 2025c). Upon its discovery in the first catalog (GWTC-1; Abbott et al. 2019; Talbot & Thrane 2018), the $35M_{\odot}$ peak was claimed to be a manifestation of the pile-up due to (pulsational) pair-instability supernovae ((P)PISNe; Woosley 2017; Spera & Mapelli 2017; Farmer et al. 2019, 2020; Ziegler & Freese 2021; Hendriks et al. 2023). The location of this pile-up in the mass spectrum has strong implications for stellar evolution theory (Belczynski et al. 2020; Stevenson et al. 2019; Golomb et al. 2024).

Previous studies have shown that a (P)PISNe peak near $30 - 40M_{\odot}$ is in tension with simulations of massive star evolution and that current understanding of the physical processes inside massive stellar cores places it at $50M_{\odot}$ or higher (see, e.g., Hendriks et al. (2023) and references therein). This has motivated alternative formation scenarios that can explain the $35M_{\odot}$ feature, such as stable mass transfer and chemically homogeneous evolution in isolated stellar binaries (de Mink & Mandel 2016; Marchant et al. 2016; Briel et al. 2023), BBHs emerging from population III stars (Kinugawa et al. 2014, 2021a,b), dynamical formation in globular clusters (GCs; Antonini et al. 2023; Ray et al. 2025; Wong et al. 2021), and hierarchical mergers (Tiwari & Fairhurst 2021; Mahapatra et al. 2025) as well as stellar mergers and accretion (Kiroğlu et al. 2025a; Kiroğlu et al. 2025c; Kremer et al. 2020) in GCs or other dense environments. Each of these scenarios can lead to unique distributions of other BBH parameters such as spins, mass ratios, and redshifts. In particular, coevolution of systems in isolated stellar binaries can lead to preferentially aligned spin components, whereas dynamical assembly leads to isotropic spin orientations (Mapelli et al. 2022; Chattopadhyay et al. 2023; Rodriguez et al. 2019, 2022) relative to the orbit (see also, Kiroğlu et al. 2025b, who show that BBH+star collisions can lead to a fraction of aligned mergers in clusters as well). Hence, to constrain the contributions of these individual formation pathways to the astrophysical population and thereby establish the origin of the $35M_{\odot}$ feature, it is necessary to identify and characterize subpopulations in the multi-dimensional BBH parameter space, including masses and spins or combinations thereof.

Several studies have investigated population-level correlations in the BBH detection sample, using both strongly modeled and non-parametric approaches. In GWTC-4, the high mass subpopulation ($\gtrsim 40M_{\odot}$) has been thoroughly investigated with both strongly modeled (e.g., Ray & Kalogera 2025; Tong et al. 2025) and semi-parametric (e.g., Antonini et al. 2025a; Wang et al. 2025) approaches. However, these works have not explored in detail the astrophysical origins of the

$35M_{\odot}$ peak. On the other hand, Banagiri et al. (2025) have parametrized the population distribution of BBH masses, component spin magnitudes, and orientations, identifying three distinct subpopulations. They find that the subpopulation in the $20 - 40M_{\odot}$ mass range has a unique mass-ratio distribution that prefers equal mass systems as compared to the other two. However, they cannot distinguish the spin distributions of this subpopulation from those of the low mass one. This can result from the low measurability of individual spin magnitudes and orientations compared to effective spin parameters or the strongly parametrized nature of their population inference.

In an earlier work, Ray et al. (2025) probed the existence of subpopulations associated with the $35M_{\odot}$ feature using a data-driven approach. By analyzing GWTC-3 BBHs using a non-parametric model for the joint distribution of BBH component masses and effective inspiral spins¹, they found evidence of a subpopulation associated with the $30 - 40M_{\odot}$ feature, which corresponds to a symmetric effective spin distribution peaking near zero. Even though effective inspiral spins can be less astrophysically interpretable compared to component spin magnitude and tilt distributions, they are not only better measured, but can also inform on whether the population is dominated by systems with spins preferentially aligned to the orbit or by ones with isotropic spin orientations. Given that a symmetric effective spin distribution about zero implies preferentially isotropic spin orientations, Ray et al. (2025) claimed, for the first time, hints of a dynamical origin of the $35M_{\odot}$ peak in GWTC-3. For a comprehensive review of which formation scenarios are likely (or unlikely) to be responsible for the $35M_{\odot}$ feature given GWTC-3 data, see Roy et al. (2025).

Repeating the analysis of Ray et al. (2025) on GWTC-4, Abac et al. (2025c) reported that the trends in the effective spin distribution of $30 - 40M_{\odot}$ BBHs have persisted as a robust feature in the updated detection sample, which comprises twice as many observations. However, *it was not explored whether the $35M_{\odot}$ feature originates exclusively from a dynamically formed subpopulation*. BBHs forming through dynamical encounters in GCs can be expected to peak in the $30 - 40M_{\odot}$ range, correspond to a symmetric effective spin distribution peaking at zero, and strongly prefer equal mass systems (Rodriguez et al. 2016; Farr et al. 2017; Antonini et al. 2023). Therefore, to ascertain whether or

¹ Effective inspiral spin is the mass-weighted sum of spins aligned with the orbital angular momentum

not BBHs in the $30 - 40M_\odot$ range are predominantly formed in GCs, it is necessary to search for such a subpopulation in the space of BBH primary (heavier component) masses, mass ratios, and effective inspiral spins, preferably with a non-parametric framework to avoid model-induced biases (Callister et al. 2022; Callister & Farr 2024; Alvarez-Lopez et al. 2025). Owing to its high flexibility and construction in the space of BBH *component masses* and effective spins, the models of Ray et al. (2025) are unable to directly constrain a subpopulation that is consistent with the effective spin and *mass-ratio* distributions predicted by BBH formation in GCs. For the same reasons, such an analysis could not assure whether the inferred mass-spin correlations are, in fact, not manifested due to an underlying mass-ratio-effective spin correlation being marginalized while reconstructing the conditional mass-spin distributions.

In this paper, using a non-parametric function for the joint distribution of BBH primary masses, mass ratios, and effective inspiral spins, constructed from binned Gaussian Processes (BGPs; Mohite 2022; Ray et al. 2023, 2025) we characterize BBH subpopulations in GWTC-4 and constrain the astrophysical origins of the $35M_\odot$ peak. We find evidence for three distinct subpopulations in the space of BBH primary masses, mass ratios and effective inspiral spins spanning the entire detection sample. We show that only one subpopulation, consistent with preferentially equal mass-systems and a symmetric effective spin distribution peaking narrowly close to zero, exhibits the $35M_\odot$ peak, whereas the other two demonstrate a monotonic fall-off in the $30 - 40M_\odot$ range. We find that the mass-spectrum of this subpopulation differs from the other two by more than 90% significance in the $30 - 40M_\odot$ range. By comparing with theoretical simulations of dynamical BBH formation in GCs, we show that only this subpopulation can comprise such systems predominantly, whereas the other two show substantial contributions from alternate channels. We conclude that, given GWTC-4, dynamical assembly in GCs likely dominates the $30 - 40M_\odot$ range and hence is a strong candidate for the origins of the $35M_\odot$ feature in the BBH mass-spectrum. We further constrain the range of BH birth-spins in GCs that are consistent with our inferred distributions.

We further find that for the lower and higher mass subpopulations, the inferred distributions are consistent with the conclusions of previous studies by Godfrey et al. (2023); Sadiq et al. (2023) and Magaña Hernandez & Palmese (2025a,b); Ray & Kalogera (2025), respectively. In particular, we find that lower masses are associated with a mass-ratio distribution peaked near $0.6 - 0.8$. For higher masses, we find that the inference can be prior driven and that flexible priors lead to no clear evidence of a PISN mass gap in agreement with the findings of Ray & Kalogera (2025). Furthermore, we do not find strong evidence of a mass-ratio-effective spin correlation in any range of primary mass. We validate our inference by exploring variations in bin resolutions and analyzing a large simulated catalog, demonstrating that our inference is not prior-driven.

The rest of this paper is organized as follows. We begin with a description of the model that we employed, in Sec. 2. In Sec. 3, we outline the main results we obtain from inference on GWTC-4 data. We discuss the astrophysical implications of our inference results in Sec. 4, concluding with a brief synopsis of the paper and future plans for improving and expanding our inference model in light of upcoming releases by the LVK from the later parts of the fourth observing run.

2. METHODS

For examining potential subpopulations in GWTC-4 data, the quantity of interest in our analysis is the merger rate density as a function of chosen parameters, i.e. the number of events for a given set of primary mass, mass ratio and effective spin of the binary. We model the rate density as a piecewise binned function in three dimensions, such that it is treated as a hyper-parameter to be inferred in each bin (Mohite 2022). Specifically, we define:

$$n^\gamma = \frac{dN^\gamma}{d \log m_1 dq d\chi_{\text{eff}} dV_c dt_s}, \quad (1)$$

where n^γ is the merger rate density per co-moving volume (V_c), source-frame time (t_s), log primary mass (m_1), mass-ratio (q) and effective spin (χ_{eff}) in the γ th bin.

Our population model permits a broad range of correlations in the $(m_1, q, \chi_{\text{eff}})$ space, and is not informed a priori by astrophysically motivated functional forms. The joint distribution takes the following form:

$$\frac{dN}{dm_1 dq dz d\chi_{\text{eff}}}(m_1, q, z, \chi_{\text{eff}} | \vec{n}, \kappa) = T_r \sum_\gamma \frac{n^\gamma}{m_1} \frac{dV_c}{dz} (1+z)^{\kappa-1} \times \begin{cases} 1 & (m_1, q, \chi_{\text{eff}}) \in \gamma^{\text{th}} \text{ bin} \\ 0 & \text{otherwise} \end{cases} \quad (2)$$

where the left-hand side represents the number of merger events per primary mass, mass ratio, effective spin and redshift; T_r is the observation time in detector frame, and κ is the redshift evolution parameter (Fishbach et al. 2018). Note that the model in Eq. 2 does not assume any particular form for the mass or spin distributions, and is flexible enough to, in principle, infer any possible correlations between parameters of interest, up to the chosen bin resolution. In addition, unphysical bins in the (m_1, q) space, i.e., bins with $q < m_{\min}/m_1$, where m_{\min} is the lowest m_1 bin, are removed to ensure that our model covers the same range of masses for both components.

The merger rate density within each bin is inferred using Bayesian hierarchical inference, with the occurrence of BBH events modeled as an inhomogeneous Poisson process (Messenger & Veitch 2013; Mandel et al. 2019; Wysocki et al. 2019; Vitale et al. 2020; Essick et al. 2025). We account for Malmquist biases in the inferred distribution using a large set of simulated signals drawn from a fiducial population. Under these considerations, we construct our rate density likelihood using observed GW data. Like previous implementations (Mohite 2022; Ray et al. 2023, 2025), the ingredients involved in constructing the rate-density likelihood have the advantage of being precomputable for a given κ value, thereby contributing to the computational efficiency of this inference framework.

The logarithmic rate density is modeled using a Gaussian process (GP) prior, which regularizes the population distribution in regions of parameter space with sparse data (Foreman-Mackey et al. 2014; Mandel et al. 2017). We use an exponential quadratic kernel to express the covariance matrix of the GP. The means, amplitude of the covariances, and correlation length scales of the GP are hyperparameters we infer simultaneously with the rate densities, and are in turn modeled using standard normal, standard half-normal, and log-normal prior distributions, respectively (Mohite 2022; Ray et al. 2023, 2025). The prior mean and variance of the length scales are chosen such that the furthest and nearest bin centers are within 4σ of the prior distribution.

To infer the joint posterior distribution of the merger rate densities and the hyperparameters describing the GP, we employ Hamiltonian Monte Carlo (HMC) sampling with the No U-Turn Sampler algorithm (Brooks et al. 2011; Hoffman & Gelman 2014). We extend the publicly available inference pipeline `gppop` (Ray et al. 2023, 2025) to implement our inference. This code in turn relies on the `PyMC` (Oriol et al. 2023) library to conduct the HMC sampling.

While constructing the population likelihood, the Monte Carlo sums used to approximate the integrals over single-event posterior samples and detectable simulations can be prone to uncertainties (Farr 2019; Essick & Farr 2022; Talbot & Golomb 2023; Heinzel & Vitale 2025), as a result of which there is a possibility of biases arising from non-converged point estimates to uncertain integrals. We monitor the variance in our likelihood function arising from that of the Monte Carlo integrals and penalize it accordingly *during sampling*, using the methods proposed by Talbot & Golomb (2023); Essick & Farr (2022); Callister & Farr (2024). This was not implemented in the previous BGP analyses of Ray et al. (2023, 2025); Hernandez & Ray (2024), where coarse bin resolutions allowed for this check to be carried out in post-processing. Further details are discussed in Appendix D.

3. RESULTS: SUBPOPULATIONS IN GWTC-4

We analyze GWTC-4 data (Abac et al. 2025b) which comprises of 153 confidently observed² BBH events (Abbott et al. 2020, 2021, 2023; Abac et al. 2025c; Essick et al. 2022), excluding clear population outliers. Due to cosmological expansion, the observed frequency/time-evolution and flux of the signal measured by the detectors get redshifted, and detector frame mass and luminosity distance samples need to be converted to source frame through a cosmological model, which we assume to be Planck2015 (Ade et al. 2016). We choose uniform in log mass bins and a specific set of χ_{eff} bins, both identical to the BGP inference of Abac et al. (2025c). For mass-ratio we choose uniform bins between 0.1 and 1. The exact locations of bin edges can be found in Table 1. To ensure that the inferred conclusions are not sensitive to binning choices, we provide inference results for an alternate bin choice with different primary mass bins in Appendix B which are fully consistent with the ones presented here.

Parameter	Bin edges
$m_1(M_\odot)$	log-uniform(5, 200, 23)
	-0.7, -0.6, -0.4, -0.3, -0.2,
χ_{eff}	-0.1, -0.05, 0.0, 0.05, 0.1, 0.15,
	0.2, 0.3, 0.4, 0.6, 0.7
q	0.1, 0.2, 0.3, 0.4, 0.5,
	0.6, 0.7, 0.8, 0.9, 1.0

Table 1. The bin choice used in this section.

² i.e., with a false alarm rate of one per year or lower.

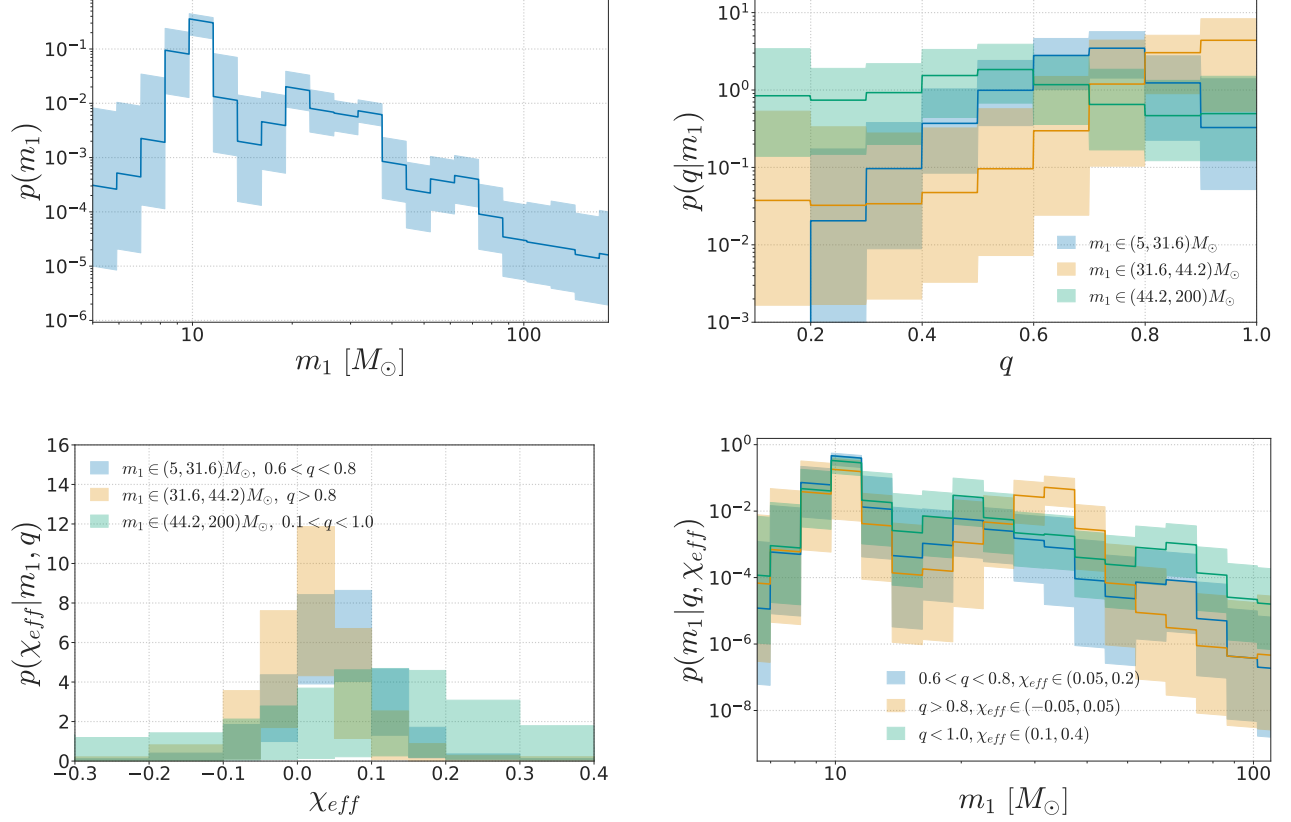


Figure 1. Marginal and conditional distributions of primary mass, mass-ratio and effective spin inferred from GWTC-4 for the bin choice described in Table 1. The top panels show the marginal primary mass distribution on the left and the mass ratio distribution conditioned on three primary mass ranges to the right. The bottom panels show the effective spin distribution for three different primary mass and mass-ratio ranges to the left and the primary mass distribution conditioned on three different mass ratio and effective spin ranges on the right.

3.1. Three distinct subpopulations

From our inferred joint distribution of BBH primary masses, mass-ratios, and effective inspiral spins, we find hints of three distinct subpopulations. Guided by the over-densities in the marginal mass-distribution, we reconstruct the conditional distribution of BBH mass-ratios given different ranges of primary mass. We then construct the inferred conditional distributions of χ_{eff} given particular ranges of primary-mass and mass-ratio. Finally, we reconstruct the conditional distribution of primary masses given mass ratio and effective spin ranges to confirm whether various features in the mass distribution indeed correspond to distinct mass ratio and effective spin distributions. Our results, displayed in Figure 1, indicate the existence of three unique BBH subpopulations in the GWTC-4 sample, which we summarize below.

- Subpopulation 1 comprises predominantly low-mass systems in the $m_1 \in (5, 31.6)M_\odot$ range displaying a sharp peak in the mass-distribution near

$10M_\odot$. It is characterized by a peak in the mass-ratio distribution in the ranges ($0.6 < q < 0.8$) and a positively skewed effective spin distribution peaked away from $\chi_{\text{eff}} = 0$, indicative of preferential alignment and non-negligible spin magnitudes. This subpopulation does not exhibit a peak in the mass distribution near $30 - 40M_\odot$.

- Subpopulation 2 contributes to the $\sim 35M_\odot$ peak in the mass distribution, is characterized by preferentially equal mass systems with the mass-ratio distribution railing against $q = 1$. It has an effective spin distribution peaked near and symmetric about $\chi_{\text{eff}} = 0$ indicating isotropic spin orientations and small spin magnitudes.
- Subpopulation 3 contributes dominantly to the higher end of the mass spectrum at $m_1 \gtrsim 40M_\odot$, has a broad, nearly flat mass-ratio distribution with support for both equal mass and asymmetric mass systems, and a broad, positively skewed effective spin distribution preferring spin alignment

and large spin magnitudes. The effective spin and mass-ratio distributions are clearly distinct from the rest of the ensemble in multiple bins with more than 90% confidence. *It also displays a peak near $60 - 70M_\odot$* (Magaña Hernandez & Palmese 2025a,b; Wang et al. 2025) and a fall off in merger rate density above $70M_\odot$.

From the reconstructed conditional mass distributions, it can be seen that only Subpopulation 2 exhibits the $35M_\odot$ peak where as the other two demonstrate a monotonic fall-off in the $30 - 40M_\odot$ mass range.

We note that a highly flexible BGP model can uncover previously unexplored trends in the population, but struggles to completely disentangle the relative abundances of specific subpopulations. Merger rate densities in a specific set of bins can only be interpreted as lower or upper bounds when compared with the theoretical predictions of a formation channel whose distributions are expected to peak in the respective ranges of the BBH parameter space. Nevertheless, the distinct features of these subpopulations can still inform on the specifics of evolutionary pathways that contribute dominantly to BBH formation in these regions of the parameter space. We discuss such astrophysical implications of our results in the context of theoretical predictions from proposed formation scenarios, as well as the results of existing subpopulation studies with GWTC-4, in Section 4.

3.2. Mass-ratio - effective spin correlation

Next we investigate the $q - \chi_{\text{eff}}$ correlation that has been reported by numerous previous works including Callister et al. (2021); Adamcewicz et al. (2023); Heinzl et al. (2024, 2025); Abac et al. (2025c). We search for this correlation not only in the entire BBH population but also in specific ranges of primary mass, which is possible from our data-driven constraints on the joint distribution of $m_1, q, \chi_{\text{eff}}$. In order to quantify the existence of this correlation, we compute the posterior distribution of the Pearson correlation coefficient between effective spin and mass ratio in different ranges of m_1 , displayed in Figure 2.

We find no significant evidence for a $q - \chi_{\text{eff}}$ correlation, either in specific mass ranges or in the entire BBH population marginalized over m_1 (see also, Roy et al. 2025, who find no evidence for a $q - \chi_{\text{eff}}$ correlation in the high mass sub-population above $20M_\odot$ using GWTC-3). We also display the median merger rate density on the two-dimensional $q - \chi_{\text{eff}}$ plane for different ranges of primary mass in Appendix A, along with the conditional distributions of χ_{eff} for different mass-ratio ranges, marginalized over primary mass. These corroborate the absence of evidence in favor of an intrinsic

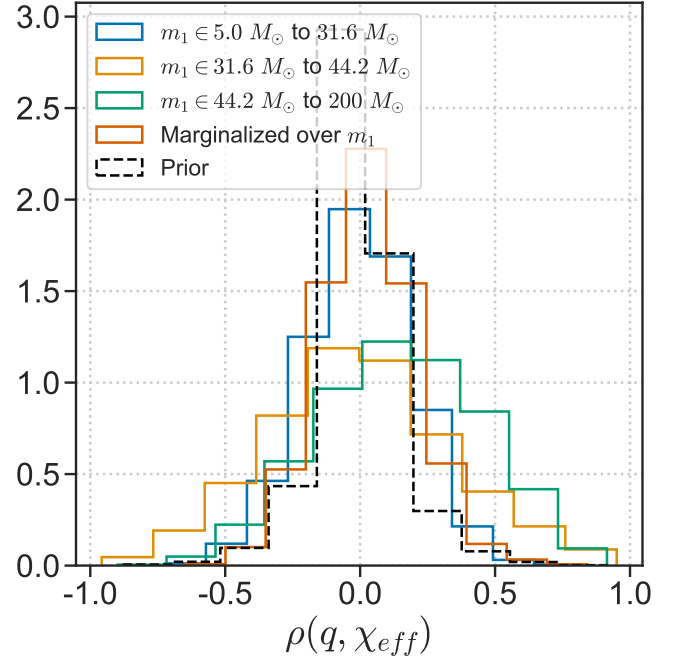


Figure 2. The Pearson correlation coefficient posteriors between effective spin and mass-ratio for three different mass ranges, namely $m_1 \in (5.0M_\odot, 31.6M_\odot)$, $m_1 \in (31.6M_\odot, 44.2M_\odot)$ and $m_1 \in (44.2M_\odot, 200M_\odot)$, along with the same marginalized across the entire primary mass space and for the prior distribution.

$q - \chi_{\text{eff}}$ correlation in the underlying population. However, given our measurement uncertainties, we do not necessarily rule out a mass-ratio and effective spin correlation and find posterior support for all values of the Pearson coefficient in the range $(-0.5, 0.5)$. Nevertheless, these results indicate that the mass-spin correlations we do find with significance are not manifesting due to marginalization over an underlying mass ratio and effective spin correlation.

4. DISCUSSION

In this work, we have resolved the joint distribution of BBH primary masses, mass ratios and effective inspiral spins using a data-driven framework for population inference based on BGP. Our examination of GWTC-4 data reveals suggestive evidence for 3 subpopulations each corresponding to a particular feature in the primary mass distribution:

1. Low primary mass ($5M_\odot < m_1 < 31.6M_\odot$) which contributes to the $\sim 10M_\odot$ peak, has a positively skewed effective spin distribution and a mass-ratio distribution peaking in the range $q \in (0.6, 0.8)$
2. Primary masses in $31.6M_\odot < m_1 < 44.2M_\odot$ which correspond to a symmetric effective spin distribu-

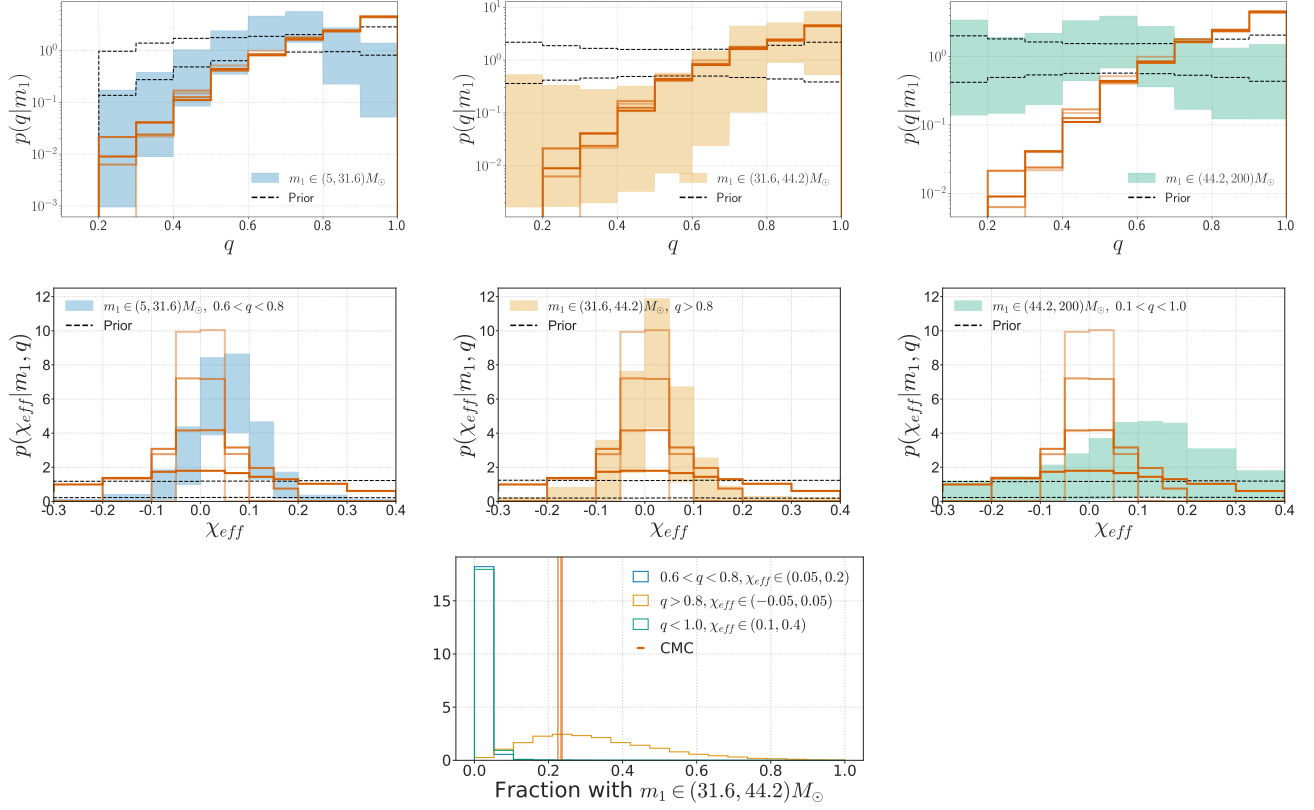


Figure 3. Comparison of conditional mass-ratio and effective spin distributions for the three subpopulations with the 1G+1G component of CMC simulations (which do not include hierarchical mergers) (Rodríguez et al. 2019). The faintest to brightest lines correspond to birth spins of 0, 0.1, 0.2 and 0.5 respectively.

tion peaking near $\chi_{\text{eff}} = 0$, and a mass-ratio distribution railing against $q = 1$; and

3. High primary masses ($m_1 > 44.2M_\odot$) corresponding to a broad effective spin distribution with a slight preference for positive values, and a broad mass-ratio distribution with a significant fraction of binaries in the range $q \in (0.6, 1)$.

By reconstructing the primary mass distributions of each subpopulation, we find that only Subpopulation 2 demonstrates the $35M_\odot$ peak, whereas the other two exhibit a monotonic fall off in $m_1 \in (20M_\odot, 50M_\odot)$. On the other hand, Subpopulation 3 exhibits hints of an overabundance in the $60 - 70M_\odot$ range and a steady fall-off afterwards. We discuss the astrophysical implications of these correlations as follows, focusing primarily on Subpopulation 2 and the origins of the $35M_\odot$ peak.

For Subpopulation 2, the symmetric effective spin distribution peaking very close to zero implies relatively equal fractions of events with aligned and anti-aligned spin orientations. Hence, it is unlikely that isolated stellar binaries, wherein co-evolution of close systems tends to align their spins to the orbit (Qin et al. 2018; Fuller & Ma 2019; Belczynski et al. 2020), contribute domi-

nantly to the subpopulation that exhibits the $\sim 35M_\odot$ peak. Similarly, the preference towards equal mass ratios makes it unlikely that BBH formation in the disks of active galactic nuclei, which is expected to have substantial support for both equal and unequal mass systems, contributes dominantly to this subpopulation (Stone et al. 2017; Bartos et al. 2017; McKernan et al. 2020). Finally, dynamically assembled systems in dense environments such as young, open, nuclear, and globular star clusters can be consistent with both the inferred effective spin and mass-ratio distributions for this subpopulation (Di Carlo et al. 2019, 2020; Rodríguez et al. 2019; Mapelli et al. 2022; Antonini & Perets 2012; Petrovich & Antonini 2017; Chattopadhyay et al. 2022). However, only GCs can explain the abundance in the $30 - 40M_\odot$ range, whereas BBH formation in nuclear and young star clusters is expected to peak at lower and higher masses, respectively (Cheng et al. 2023; Antonini et al. 2023; Mapelli et al. 2022). From this, we conclude that the $35M_\odot$ feature likely arises due to a dynamically formed subpopulation of BBHs originating in GCs. While previous studies have reported *hints* of this conclusion in the data from earlier catalogs (Ray et al. 2025), our data-driven reconstruction of the BBH primary mass,

mass-ratio, and effective spin distribution from GWTC-4 demonstrates stronger evidence.

However, BBHs formed in GCs can, in principle, also contribute to the other two subpopulations. Furthermore, the predicted distributions can be susceptible to theoretical uncertainties such as the distribution of BH birth spins. In Figure 3, we compare the subpopulations we uncovered with star cluster (Rodríguez et al. 2019) simulations derived from publicly available Cluster Monte Carlo (CMC; Pattabiraman et al. 2013) code. The simulations were taken from the public data release by Zevin (2020). The simulated systems only comprise first generational mergers and correspond to the 4 specific values of BH birth spin. We find that *only Subpopulation 2 is fully consistent (at the 90% level of the inferred distributions) with these theoretical predictions*. We further find that *only the simulations that correspond to BH birth spins in the range 0.1 – 0.2, are consistent*, and that higher or lower values lead to an effective spin distribution that is either too broad or too narrow, respectively, as compared to the inferred one. Furthermore, the fraction of systems in the $30 - 40M_{\odot}$ range for the simulated populations is only consistent with that inferred from Subpopulation 2 and inconsistent with the other two. In other words, given GWTC-4, we find that *dynamical mergers in GCs can contribute predominantly only in the $30 - 40M_{\odot}$ range*, whereas the subpopulations in other mass ranges have significant contributions from alternate formation channels. The merger rate in this mass range, therefore, serves as a lower bound on that of dynamically assembled BBHs in GCs, which we constrain to be $0.69^{+0.23}_{-0.33} \text{Gpc}^{-3} \text{yr}^{-1}$.

Note that the mass distribution of dynamically formed BBHs in GCs need not exhibit a sharp peak near $35M_{\odot}$ itself to produce the observed feature. Even a broad mass distribution that falls off sharply above $\sim 40M_{\odot}$ can explain the inferred distribution. We argue that the $35M_{\odot}$ feature can arise in the inferred distributions due to alternative formation channels (that dominate at lower masses) becoming subdominant to GCs in the $30 - 40M_{\odot}$ range. In such a scenario, even a nearly flat mass distribution from the GC channel that falls off rapidly above $40M_{\odot}$, can give rise to a bump in the $30 - 40M_{\odot}$ range relative to the rest of the mass-spectrum. Our inferred mass-ratio and effective spin distributions are fully consistent with this hypothesis. In other words, our conclusion regarding the astrophysical origin of Subpopulation 2 and the $35M_{\odot}$ feature is robust against uncertainties in the shape of the mass-spectrum of BBHs formed in GCs, as long as substantial support is expected in the $30 - 40M_{\odot}$ mass-range.

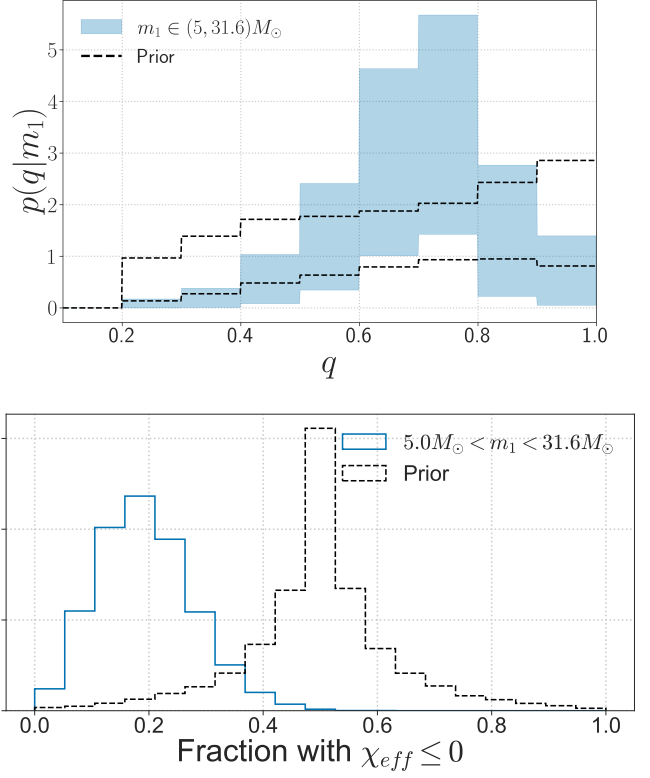


Figure 4. The mass-ratio distribution (top) and fraction of events with $\chi_{\text{eff}} < 0$ (bottom) for the low-mass ($m_1 < 30M_{\odot}$) subpopulation.

Next, we turn to Subpopulation 1, whose positively skewed effective spin distribution peaking away from zero implies preference towards aligned systems and non-negligible spin magnitudes. This is consistent with the predictions of isolated binary evolution (Fuller & Ma 2019; Zevin & Bavera 2022; Briel et al. 2023). Previous investigations have shown that the $10M_{\odot}$ peak can arise from the stable mass transfer in isolated stellar binaries and that it is robust against several uncertainties in theoretical modeling (van Son et al. 2023, 2022a). Furthermore, mass-ratio reversal during stable mass-transfer can lead to a preference towards unequal mass-ratios in the range $q \in (0.6, 0.8)$ (Neijssel et al. 2019; van Son et al. 2022b; Broekgaarden et al. 2022; Mould et al. 2022; Adamcewicz et al. 2024; Biscoveanu 2025). The prominent peak near mass-ratios $0.6 - 0.8$ and a suppressed fraction of $\chi_{\text{eff}} \leq 0$ systems in our inferred distributions of Subpopulation 1 (as shown in Figure 4) can therefore be indicative of substantial contributions from isolated binary evolution through stable mass transfer. However, our findings do not rule out the hypothesis that alternate pathways of isolated BBH formation contribute dominantly or substantially to Subpopulation 1.

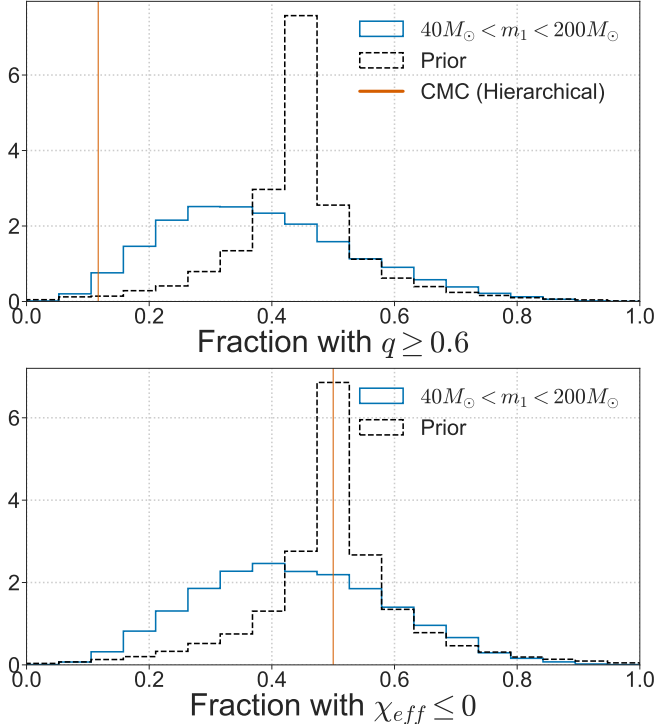


Figure 5. Fraction of events with $q > 0.6$ (top) and $\chi_{\text{eff}} < 0$ (bottom) for the high-mass ($m_1 > 40M_{\odot}$) subpopulation. The orange line represents all hierarchical mergers from the simulations of Rodriguez et al. (2019), with the models corresponding to each BH birth spin combined with equal weightage.

Our findings for Subpopulation 3 are broadly consistent with previous studies that have explored trends in high-mass BBHs in GWTC-4 (Banagiri et al. 2025; Wang et al. 2025; Ray & Kalogera 2025). In particular, we find that for masses $\gtrsim 40M_{\odot}$, there is a broadening of the χ_{eff} distribution (Antonini et al. 2025a,b,c) and evidence of a flat mass-ratio distribution that is in alignment with the findings of Ray & Kalogera (2025). Figure 5 (top and bottom) shows the fraction of events with $q > 0.6$ and $\chi_{\text{eff}} < 0$ respectively, for Subpopulation 3. The inferred fractions indicate substantial contributions from alternative formation scenarios to hierarchical mergers. Potential scenarios include but are not limited to Super Eddington accretion during mass-transfer, chemically homogeneous evolution, population III stars, and accretion-driven growth after BH+Star collisions in dense environments (Briel et al. 2023; van Son et al. 2023; de Mink & Mandel 2016; Kinugawa et al. 2021b; Kiroğlu et al. 2025c). The hints of a peak in the $60 - 70M_{\odot}$ mass range for this subpopulation (and in the marginal m_1 distribution) might be indicative of the pile-up due to (P)PISNe, although, given the large error-bars, more data might be needed to confirm this

conclusion. We note however that unlike Subpopulations 1 and 2, the high mass region is more strongly influenced by the prior in several parts of the q and χ_{eff} parameter spaces. Furthermore, flexible priors such as the one used in this work and the ones used by Ray & Kalogera (2025) lead to inferred distributions that exhibit no clear evidence of a PISN mass gap.

Moving forward, the growing number of detections made by the LVK as part of their latest observing run will be vital to further tighten constraints on the nature of BBH subpopulations. To confirm a dynamical origin of the $35M_{\odot}$ peak it is necessary to simultaneously model the distribution of effective precessing spins, since the χ_{eff} distributions can only inform on the fraction of alignment vs anti-alignment, and not on mis-alignment/precession, which is expected to be substantial in dynamically assembled binaries (Gerosa & Fishbach 2021; Payne et al. 2024). Focused investigations for other subpopulations, such as the $20M_{\odot}$ peak, should it persist in updated catalogs, are also expected to be more feasible. A generic characterization of BBH subpopulations using higher-dimensional BGP models from future catalogs is left as an upcoming exploration.

As noted before, a BGP-based framework, while preferable to search for previously unmodeled features and correlations in the BBH population, might not be optimal to completely isolate these clusters in the parameter space. Furthermore, the sampling techniques necessitated by such complex models do not yield Bayesian evidences, which makes it difficult to rigorously ascertain how much the data prefers the existence of these specific subpopulations. To isolate the contributions of specific subpopulations, compute merger rates that are directly comparable to theoretical simulations of specific formation channels, and perform model comparison, it is necessary to develop and constrain targeted parametrizations of the BBH population distribution guided by the trends uncovered through the non-parametric inference presented here. Such an investigation with GWTC-4 data is ongoing and will be communicated in the near future.

5. ACKNOWLEDGEMENTS

We are thankful to Mike Zevin and Tom Dent for insightful discussions and suggestions. A.R. was supported by the National Science Foundation (NSF) award PHY-2207945. V.K. was supported by the Gordon and Betty Moore Foundation (grant awards GBMF8477 and GBMF12341), through a Guggenheim Fellowship, and the D.I. Linzer Distinguished University Professorship fund. We are grateful for the computational resources provided by the LIGO laboratory and supported by

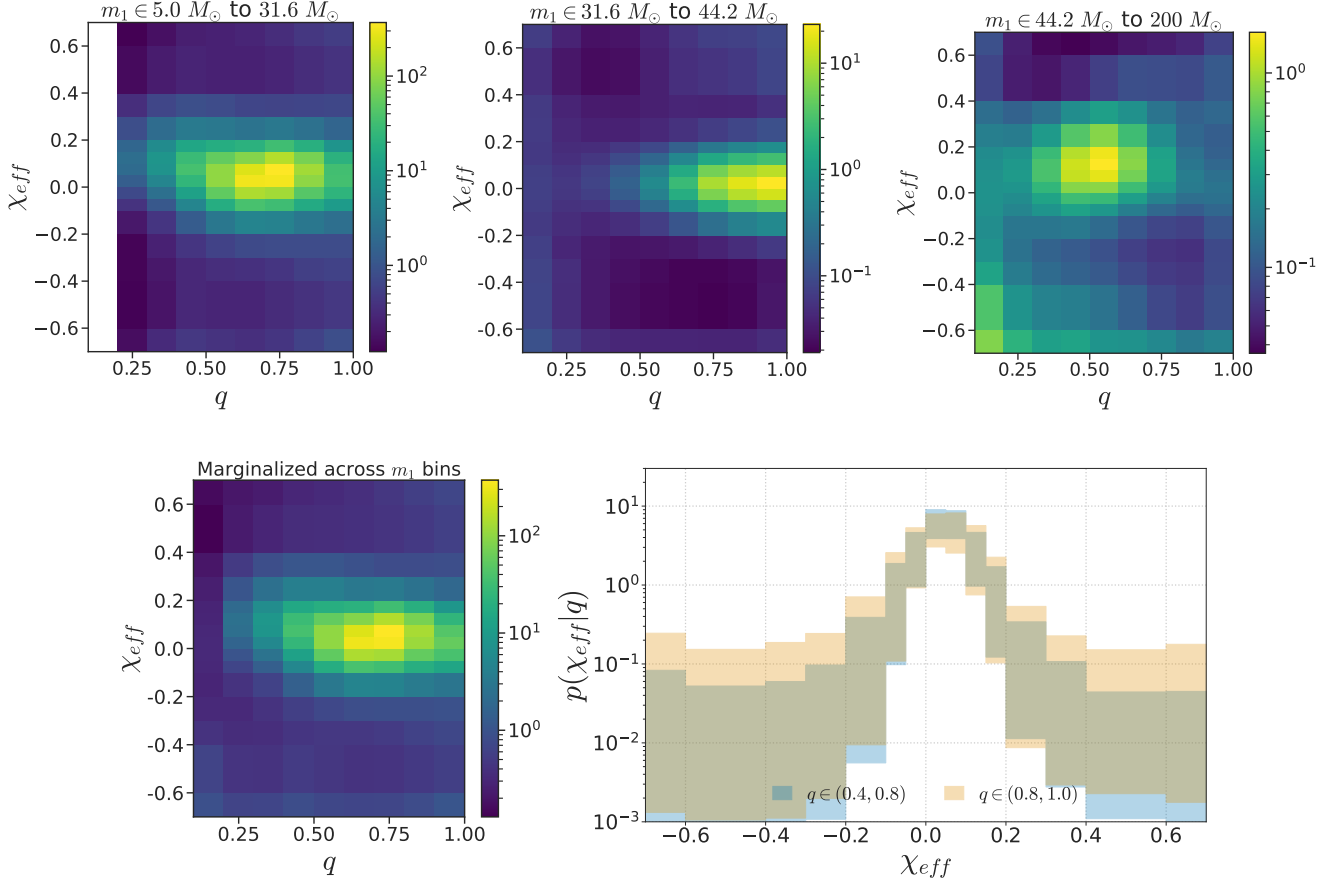


Figure 6. Inferred distributions highlighting the absence of support for a correlation between mass-ratio and effective spin. The top panels display 2d slices of the median merger rate density distribution obtained from GWTC-4, for the three primary mass ranges as in Figure 2. The bottom left panel shows the same but for the mass-marginalized case. The bottom right panel represents the χ_{eff} distribution for different ranges of mass-ratio.

National Science Foundation Grants PHY-0757058 and PHY-0823459. This material is based upon work supported by NSF’s LIGO Laboratory, which is a major facility fully funded by the National Science Foundation. This research has made use of data obtained from the gravitational Wave Open Science Center (gwosc.org), a service of LIGO Laboratory, the LIGO Scientific Collaboration, the Virgo Collaboration, and KAGRA. A.R.

and V.K. gratefully acknowledge the support of the NSF-Simons AI-Institute for the Sky (SkAI) via grants NSF AST-2421845 and Simons Foundation MPS-AI-00010513. This research was supported in part through the computational resources and staff contributions provided for the Quest high performance computing facility at Northwestern University which is jointly supported by the Office of the Provost, the Office for Research, and Northwestern University Information Technology.

APPENDIX

A. MASS-RATIO AND EFFECTIVE SPIN DISTRIBUTIONS

We display the two-dimensional median merger rate density distributions in Figure 6. They corroborate the conclusions from the Pearson posteriors in Figure 2 of an absence of (q, χ_{eff}) correlations in any of the primary mass ranges of interest.

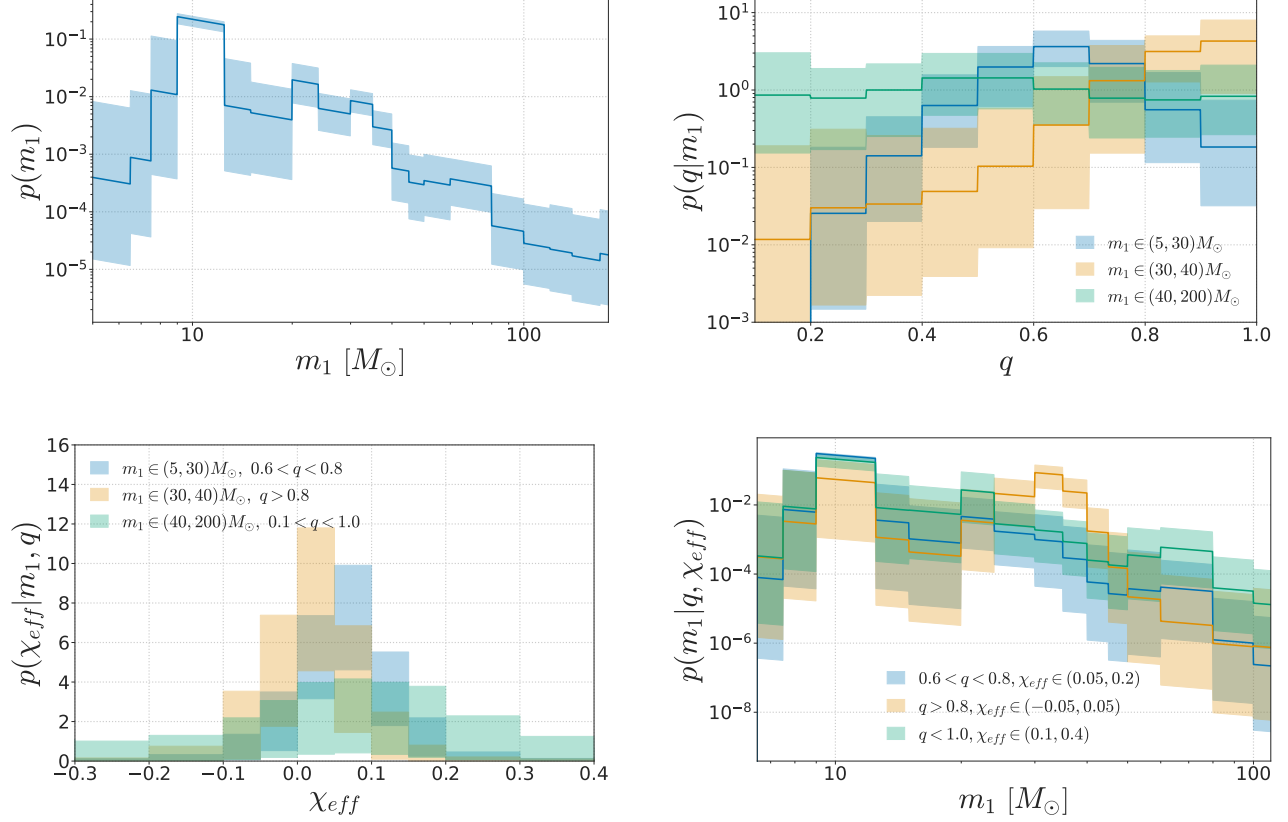


Figure 7. Marginal and conditional distributions of primary mass, mass-ratio and effective spin inferred from GWTC-4 for an alternate bin choice with non-uniform primary mass bins.

B. VARIATION OF BINNING CHOICE

We show in Figure 7 the inference trends we find for GWTC-4 for a different bin choice with non-uniform primary mass bins (see Table 2). We recover results consistent with those presented in Sec. 3.1 and Sec. 4, thereby confirming that the subpopulations are robust against bin variations.

Parameter	Bin edges
$m_1 (M_\odot)$	5, 6.5, 7.5, 9, 12.5, 15, 20, 24, 30, 35, 40, 45, 50, 60, 80, 100, 120, 140, 170, 200
χ_{eff}	-0.7, -0.6, -0.4, -0.3, -0.2, -0.1, -0.05, 0.0, 0.05, 0.1, 0.15, 0.2, 0.3, 0.4, 0.6, 0.7
q	0.1, 0.2, 0.3, 0.4, 0.5, 0.6, 0.7, 0.8, 0.9, 1.0

Table 2. The non uniform mass bin choice used in Figure 7

C. VALIDATION OF RESULTS WITH UNCORRELATED SIMULATION

To ensure that the correlations we determine by inferring the joint hyperposterior are not manifesting out of artifacts built into our model, we validate our results using a simulated population that does not contain any intrinsic correlations in the $(m_1, q, \chi_{\text{eff}})$ space. This is achieved by independently drawing binary parameters from the uncorrelated population distribution and thereafter injecting these signals into synthetic detector noise, and finally passing them through the same selection and analysis pipeline as the real data. In order to perform event level parameter estimation on these injections, we employ Bayesian inference using the BILBY package (Ashton et al. 2019; Romero-Shaw et al. 2020), its multi-purpose nested sampler DYNesty (Speagle 2020), and the IMRphenomD aligned spin waveform approximant (Husa et al. 2016; Khan et al. 2016). By comparing the inferred correlations (or lack thereof) recovered

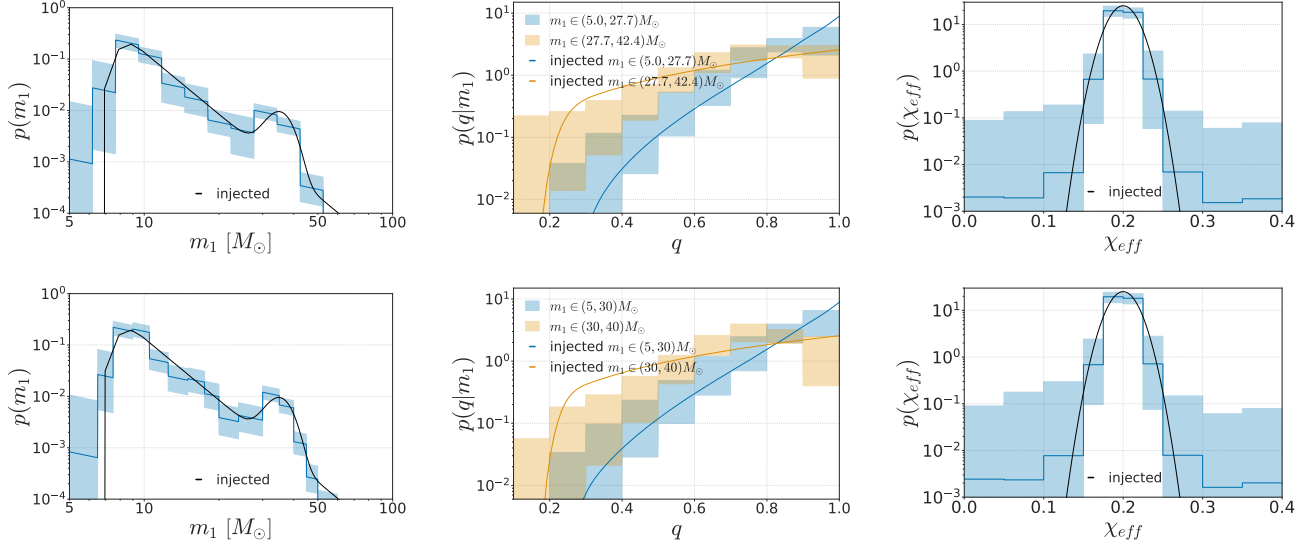


Figure 8. Marginal and conditional distributions of BBH primary mass, mass ratio and effective spin for the simulated catalog with no intrinsic correlations between the three parameters, for two different m_1 bin resolutions (log uniform on top and a non-uniform choice at the bottom).

from this control population to those observed in the actual LVK data, we assess whether the empirical correlations are driven by model systematics or are statistically significant features of the underlying astrophysical population.

Upon conducting population inference using our framework on this simulated dataset, we find that the subpopulation trends recovered from the GWTC-4 event set are not a result of biases built into the model. The marginal primary mass, conditional mass-ratio with respect to primary mass, and marginal effective spin distributions (Figure 8) recovered by our model are consistent with the true injected distributions. We have therefore verified that the predictions we make regarding the GWTC-4 data are not spuriously arising due to model artifacts.

D. CONVERGENCE OF MONTE CARLO INTEGRALS

The Monte Carlo sums used to approximate the integrals over the posterior samples can be prone to uncertainties as a result of which there is a possibility of issues relating to convergence of samples.

The implementation of the event-specific posterior bin supports and detectable time-volumes (see Ray et al. (2023)) includes the computation of the means and variances of the same. The effective sample size for both detectable injections and event-specific posteriors is determined from their means and standard deviations, using $N_{\text{eff}} = \left(\frac{\mu}{\sigma}\right)^2$. It must be sufficiently large to prevent biases in the inferred hyperparameters caused by the above-mentioned Monte Carlo uncertainties. Following the description of convergence testing provided in Appendix A of Hernandez & Ray (2024), we therefore require the following conditions to be satisfied-

$$\frac{N_{\text{eff}}^{\text{VT}}(\Lambda)}{N_{\text{det}}(\vec{n}, \Lambda)} = \frac{\sum_{\gamma, \alpha} \left(\frac{\mu_{\text{VT}}^{\gamma\alpha}}{\sigma_{\text{VT}}^{\gamma\alpha}} \right)^2}{\sum_{\gamma, \alpha} n^{\gamma} \mu_{\text{VT}}^{\gamma\alpha}} \geq 2 \quad (\text{D1})$$

$$\min_i N_{\text{eff}}^{w,i}(\vec{n}, \Lambda) = \min_i \left\{ \frac{\left(\sum_{\gamma, \alpha} n^{\gamma} \mu_{w,i}^{\gamma\alpha} \right)^2}{\sum_{\gamma, \alpha} (n^{\gamma} \sigma_{w,i}^{\gamma\alpha})^2} \right\} \geq 10^{0.6} \quad (\text{D2})$$

for all hypersamples at each Monte Carlo sampling step, with $N_{\text{eff}}^{\text{VT}}$, N_{det} , $N_{\text{eff}}^{w,i}$ being the effective number of injected samples, number of observed events and effective number of posterior samples informing the likelihood respectively. This has indeed been verified, and samples that did not rigorously satisfy these conditions were deleted at the inference stage, by using a step function framework (Essick & Farr 2022; Callister & Farr 2024) that rejects samples that fail to follow the convergence criteria. Callister & Farr (2024) define a function-

$$\mathcal{S}(x) = \frac{1}{1 + x^{-30}} \quad (\text{D3})$$

which asymptotically approaches zero for $x \rightarrow 0$ and unity for large x . The log-likelihood therefore takes the following form-

$$\log p(\vec{d}|\vec{n}) = - \sum_{\gamma} n^{\gamma} \langle VT \rangle^{\gamma} + \sum_i \log \left(\sum_{\gamma} n^{\gamma} w^{\gamma}(d_i) \right) + \ln \mathcal{S}(N_{\text{eff}}^{\text{VT}}/2N_{\text{det}}) + \ln \mathcal{S}(\min_i \log_{10} N_{\text{eff}}^{w,i}/0.6) \quad (\text{D4})$$

REFERENCES

- Aasi, J., et al. 2015, *Class. Quant. Grav.*, 32, 074001, doi: [10.1088/0264-9381/32/7/074001](https://doi.org/10.1088/0264-9381/32/7/074001)
- Abac, A. G., et al. 2025a. <https://arxiv.org/abs/2508.18082>
- . 2025b. <https://arxiv.org/abs/2508.18079>
- . 2025c. <https://arxiv.org/abs/2508.18083>
- Abbott, B. P., et al. 2019, *Phys. Rev. X*, 9, 031040, doi: [10.1103/PhysRevX.9.031040](https://doi.org/10.1103/PhysRevX.9.031040)
- Abbott, R., Abbott, T. D., Abraham, S., et al. 2020, *The Astrophysical Journal Letters*, 896, L44, doi: [10.3847/2041-8213/ab960f](https://doi.org/10.3847/2041-8213/ab960f)
- . 2021, *The Astrophysical Journal Letters*, 913, L7, doi: [10.3847/2041-8213/abe949](https://doi.org/10.3847/2041-8213/abe949)
- . 2023, *Physical Review X*, 13, 011048, doi: [10.1103/PhysRevX.13.011048](https://doi.org/10.1103/PhysRevX.13.011048)
- Acernese, F., Agathos, M., Agatsuma, K., et al. 2014, *Classical and Quantum Gravity*, 32, 024001, doi: [10.1088/0264-9381/32/2/024001](https://doi.org/10.1088/0264-9381/32/2/024001)
- Adamcewicz, C., Galaudage, S., Lasky, P. D., & Thrane, E. 2024, *Astrophys. J. Lett.*, 964, L6, doi: [10.3847/2041-8213/ad2df2](https://doi.org/10.3847/2041-8213/ad2df2)
- Adamcewicz, C., Lasky, P. D., & Thrane, E. 2023, *The Astrophysical Journal*, 956, 63, doi: [10.3847/1538-4357/acf763](https://doi.org/10.3847/1538-4357/acf763)
- Ade, P. A. R., et al. 2016, *Astron. Astrophys.*, 594, A13, doi: [10.1051/0004-6361/201525830](https://doi.org/10.1051/0004-6361/201525830)
- Akutsu, T., Ando, M., Arai, K., et al. 2021, *Progress of Theoretical and Experimental Physics*, 2021, 05A102, doi: [10.1093/ptep/ptab018](https://doi.org/10.1093/ptep/ptab018)
- Alvarez-Lopez, S., Heinzl, J., Mould, M., & Vitale, S. 2025. <https://arxiv.org/abs/2506.20731>
- Antonini, F., Callister, T., Dosopoulou, F., Romero-Shaw, I. M., & Chattopadhyay, D. 2025a, *Phys. Rev. D*, 112, 063040, doi: [10.1103/nxnr-pdyx](https://doi.org/10.1103/nxnr-pdyx)
- Antonini, F., Gieles, M., Dosopoulou, F., & Chattopadhyay, D. 2023, *Monthly Notices of the Royal Astronomical Society*, 522, 466, doi: [10.1093/mnras/stad972](https://doi.org/10.1093/mnras/stad972)
- Antonini, F., & Perets, H. B. 2012, *Astrophys. J.*, 757, 27, doi: [10.1088/0004-637X/757/1/27](https://doi.org/10.1088/0004-637X/757/1/27)
- Antonini, F., Romero-Shaw, I., Callister, T., et al. 2025b. <https://arxiv.org/abs/2509.04637>
- Antonini, F., Romero-Shaw, I. M., & Callister, T. 2025c, *Phys. Rev. Lett.*, 134, 011401, doi: [10.1103/PhysRevLett.134.011401](https://doi.org/10.1103/PhysRevLett.134.011401)
- Ashton, G., Hübner, M., Lasky, P. D., et al. 2019, *The Astrophysical Journal Supplement Series*, 241, 27, doi: [10.3847/1538-4365/ab06fc](https://doi.org/10.3847/1538-4365/ab06fc)
- Banagiri, S., Thrane, E., & Lasky, P. D. 2025. <https://arxiv.org/abs/2509.15646>
- Bartos, I., Kocsis, B., Haiman, Z., & Márka, S. 2017, *Astrophys. J.*, 835, 165, doi: [10.3847/1538-4357/835/2/165](https://doi.org/10.3847/1538-4357/835/2/165)
- Belczynski, K., Kalogera, V., & Bulik, T. 2001, *Astrophys. J.*, 572, 407, doi: [10.1086/340304](https://doi.org/10.1086/340304)
- Belczynski, K., et al. 2020, *Astron. Astrophys.*, 636, A104, doi: [10.1051/0004-6361/201936528](https://doi.org/10.1051/0004-6361/201936528)
- Biscoveanu, S. 2025. <https://arxiv.org/abs/2502.04278>
- Briel, M. M., Stevance, H. F., & Eldridge, J. J. 2023, *Mon. Not. Roy. Astron. Soc.*, 520, 5724, doi: [10.1093/mnras/stad399](https://doi.org/10.1093/mnras/stad399)
- Broekgaarden, F. S., Stevenson, S., & Thrane, E. 2022, *Astrophys. J.*, 938, 45, doi: [10.3847/1538-4357/ac8879](https://doi.org/10.3847/1538-4357/ac8879)
- Brooks, S., Gelman, A., Jones, G., & Meng, X.-L. 2011, *Handbook of Markov Chain Monte Carlo* (Chapman and Hall/CRC), doi: [10.1201/b10905](https://doi.org/10.1201/b10905)
- Callister, T. A., & Farr, W. M. 2024, *Phys. Rev. X*, 14, 021005, doi: [10.1103/PhysRevX.14.021005](https://doi.org/10.1103/PhysRevX.14.021005)
- Callister, T. A., Haster, C.-J., Ng, K. K. Y., Vitale, S., & Farr, W. M. 2021, *The Astrophysical Journal Letters*, 922, L5, doi: [10.3847/2041-8213/ac2ccc](https://doi.org/10.3847/2041-8213/ac2ccc)
- Callister, T. A., Miller, S. J., Chatziioannou, K., & Farr, W. M. 2022, *Astrophys. J. Lett.*, 937, L13, doi: [10.3847/2041-8213/ac847e](https://doi.org/10.3847/2041-8213/ac847e)
- Chattopadhyay, D., Hurley, J., Stevenson, S., & Raidani, A. 2022, *MNRAS*, 513, 4527, doi: [10.1093/mnras/stac1163](https://doi.org/10.1093/mnras/stac1163)

- Chattopadhyay, D., Stegmann, J., Antonini, F., Barber, J., & Romero-Shaw, I. M. 2023, *Mon. Not. Roy. Astron. Soc.*, 526, 4908, doi: [10.1093/mnras/stad3048](https://doi.org/10.1093/mnras/stad3048)
- Cheng, A. Q., Zevin, M., & Vitale, S. 2023, *Astrophys. J.*, 955, 127, doi: [10.3847/1538-4357/aced98](https://doi.org/10.3847/1538-4357/aced98)
- de Mink, S. E., & Mandel, I. 2016, *Mon. Not. Roy. Astron. Soc.*, 460, 3545, doi: [10.1093/mnras/stw1219](https://doi.org/10.1093/mnras/stw1219)
- Di Carlo, U. N., Giacobbo, N., Mapelli, M., et al. 2019, *Mon. Not. Roy. Astron. Soc.*, 487, 2947, doi: [10.1093/mnras/stz1453](https://doi.org/10.1093/mnras/stz1453)
- Di Carlo, U. N., et al. 2020, *Mon. Not. Roy. Astron. Soc.*, 498, 495, doi: [10.1093/mnras/staa2286](https://doi.org/10.1093/mnras/staa2286)
- Doctor, Z., Wysocki, D., O’Shaughnessy, R., Holz, D. E., & Farr, B. 2020, *The Astrophysical Journal*, 893, 35, doi: [10.3847/1538-4357/ab7fac](https://doi.org/10.3847/1538-4357/ab7fac)
- Essick, R., Farah, A., Galaudage, S., et al. 2022, *The Astrophysical Journal*, 926, 34, doi: [10.3847/1538-4357/ac3978](https://doi.org/10.3847/1538-4357/ac3978)
- Essick, R., & Farr, W. 2022, arXiv preprint arXiv:2204.00461. <https://arxiv.org/abs/2204.00461>
- Essick, R., et al. 2025, *Phys. Rev. D*, 112, 102001, doi: [10.1103/44x3-hv3y](https://doi.org/10.1103/44x3-hv3y)
- Farmer, R., Renzo, M., de Mink, S., Fishbach, M., & Justham, S. 2020, *Astrophys. J. Lett.*, 902, L36, doi: [10.3847/2041-8213/abbadd](https://doi.org/10.3847/2041-8213/abbadd)
- Farmer, R., Renzo, M., de Mink, S. E., Marchant, P., & Justham, S. 2019, *The Astrophysical Journal*, 887, 53, doi: [10.3847/1538-4357/ab518b](https://doi.org/10.3847/1538-4357/ab518b)
- Farr, W. M. 2019, *Research Notes of the AAS*, 3, 66, doi: [10.3847/2515-5172/ab1d5f](https://doi.org/10.3847/2515-5172/ab1d5f)
- Farr, W. M., Stevenson, S., Coleman Miller, M., et al. 2017, *Nature*, 548, 426, doi: [10.1038/nature23453](https://doi.org/10.1038/nature23453)
- Fishbach, M., Holz, D. E., & Farr, B. 2017, *The Astrophysical Journal Letters*, 840, L24, doi: [10.3847/2041-8213/aa7045](https://doi.org/10.3847/2041-8213/aa7045)
- Fishbach, M., Holz, D. E., & Farr, W. M. 2018, *Astrophys. J. Lett.*, 863, L41, doi: [10.3847/2041-8213/aaf9a4](https://doi.org/10.3847/2041-8213/aaf9a4)
- Foreman-Mackey, D., Hogg, D. W., & Morton, T. D. 2014, *The Astrophysical Journal*, 795, 64, doi: [10.1088/0004-637X/795/1/64](https://doi.org/10.1088/0004-637X/795/1/64)
- Fuller, J., & Ma, L. 2019, *Astrophys. J. Lett.*, 881, L1, doi: [10.3847/2041-8213/ab339b](https://doi.org/10.3847/2041-8213/ab339b)
- Gerosa, D., & Berti, E. 2017, *Phys. Rev. D*, 95, 124046, doi: [10.1103/PhysRevD.95.124046](https://doi.org/10.1103/PhysRevD.95.124046)
- Gerosa, D., & Fishbach, M. 2021, *Nature Astron.*, 5, 749, doi: [10.1038/s41550-021-01398-w](https://doi.org/10.1038/s41550-021-01398-w)
- Godfrey, J., Edelman, B., & Farr, B. 2023, *Cosmic Cousins: Identification of a Subpopulation of Binary Black Holes Consistent with Isolated Binary Evolution*. <https://arxiv.org/abs/2304.01288>
- Golomb, J., Isi, M., & Farr, W. M. 2024, *Astrophys. J.*, 976, 121, doi: [10.3847/1538-4357/ad8572](https://doi.org/10.3847/1538-4357/ad8572)
- Heinzel, J., Biscoveanu, S., & Vitale, S. 2024, *Phys. Rev. D*, 109, 103006, doi: [10.1103/PhysRevD.109.103006](https://doi.org/10.1103/PhysRevD.109.103006)
- Heinzel, J., Mould, M., & Vitale, S. 2025, *Phys. Rev. D*, 111, L061305, doi: [10.1103/PhysRevD.111.L061305](https://doi.org/10.1103/PhysRevD.111.L061305)
- Heinzel, J., & Vitale, S. 2025. <https://arxiv.org/abs/2509.07221>
- Hendriks, D. D., van Son, L. A. C., Renzo, M., Izzard, R. G., & Farmer, R. 2023, *Mon. Not. Roy. Astron. Soc.*, 526, 4130, doi: [10.1093/mnras/stad2857](https://doi.org/10.1093/mnras/stad2857)
- Hernandez, I. M., & Ray, A. 2024, arXiv preprint arXiv:2404.02522. <https://arxiv.org/abs/2404.02522>
- Hoffman, M. D., & Gelman, A. 2014, *Journal of Machine Learning Research*, 15, 1593. <https://www.jmlr.org/papers/volume15/hoffman14a/hoffman14a.pdf>
- Husa, S., Khan, S., Hannam, M., et al. 2016, *Phys. Rev. D*, 93, 044006, doi: [10.1103/PhysRevD.93.044006](https://doi.org/10.1103/PhysRevD.93.044006)
- Khan, S., Husa, S., Hannam, M., et al. 2016, *Phys. Rev. D*, 93, 044007, doi: [10.1103/PhysRevD.93.044007](https://doi.org/10.1103/PhysRevD.93.044007)
- Kimball, C., et al. 2021, *Astrophys. J. Lett.*, 915, L35, doi: [10.3847/2041-8213/ac0aef](https://doi.org/10.3847/2041-8213/ac0aef)
- Kinugawa, T., Inayoshi, K., Hotokezaka, K., Nakauchi, D., & Nakamura, T. 2014, *Mon. Not. Roy. Astron. Soc.*, 442, 2963, doi: [10.1093/mnras/stu1022](https://doi.org/10.1093/mnras/stu1022)
- Kinugawa, T., Nakamura, T., & Nakano, H. 2021a, *Mon. Not. Roy. Astron. Soc.*, 501, L49, doi: [10.1093/mnrasl/slaa191](https://doi.org/10.1093/mnrasl/slaa191)
- . 2021b, *Mon. Not. Roy. Astron. Soc.*, 504, L28, doi: [10.1093/mnrasl/slab032](https://doi.org/10.1093/mnrasl/slab032)
- Kiroğlu, F., Lombardi, J. C., Kremer, K., Vanderzyden, H. D., & Rasio, F. A. 2025b, *Astrophys. J. Lett.*, 983, L9, doi: [10.3847/2041-8213/adc263](https://doi.org/10.3847/2041-8213/adc263)
- Kiroğlu, F., Kremer, K., Biscoveanu, S., González Prieto, E., & Rasio, F. A. 2025a, *Astrophys. J.*, 979, 237, doi: [10.3847/1538-4357/ada26b](https://doi.org/10.3847/1538-4357/ada26b)
- Kremer, K., Spera, M., Becker, D., et al. 2020, *Astrophys. J.*, 903, 45, doi: [10.3847/1538-4357/abb945](https://doi.org/10.3847/1538-4357/abb945)
- Kulkarni, S. F., McMillan, S., & Hut, P. 1993, *Nature*, 364, 421, doi: [10.1038/364421a0](https://doi.org/10.1038/364421a0)
- Kiroğlu, F., Kremer, K., & Rasio, F. A. 2025c, *Astrophys. J. Lett.*, 994, L37, doi: [10.3847/2041-8213/ae1eeb](https://doi.org/10.3847/2041-8213/ae1eeb)
- Magaña Hernandez, I., & Palmese, A. 2025a, *Phys. Rev. D*, 111, 083031, doi: [10.1103/PhysRevD.111.083031](https://doi.org/10.1103/PhysRevD.111.083031)
- . 2025b. <https://arxiv.org/abs/2508.19208>
- Mahapatra, P., Chattopadhyay, D., Gupta, A., et al. 2025, *Phys. Rev. D*, 111, 023013, doi: [10.1103/PhysRevD.111.023013](https://doi.org/10.1103/PhysRevD.111.023013)

- Mandel, I., Farr, W. M., Colonna, A., et al. 2017, *Monthly Notices of the Royal Astronomical Society*, 465, 3254, doi: [10.1093/mnras/stw2883](https://doi.org/10.1093/mnras/stw2883)
- Mandel, I., Farr, W. M., & Gair, J. R. 2019, *Monthly Notices of the Royal Astronomical Society*, 486, 1086, doi: [10.1093/mnras/stz2896](https://doi.org/10.1093/mnras/stz2896)
- Mapelli, M., Bouffanais, Y., Santoliquido, F., Sedda, M. A., & Artale, M. C. 2022, *Mon. Not. Roy. Astron. Soc.*, 511, 5797, doi: [10.1093/mnras/stac422](https://doi.org/10.1093/mnras/stac422)
- Marchant, P., Langer, N., Podsiadlowski, P., Tauris, T. M., & Moriya, T. J. 2016, *Astron. Astrophys.*, 588, A50, doi: [10.1051/0004-6361/201628133](https://doi.org/10.1051/0004-6361/201628133)
- McKernan, B., Ford, K. E. S., O’Shaughnessy, R., & Wysocki, D. 2020, *Mon. Not. Roy. Astron. Soc.*, 494, 1203, doi: [10.1093/mnras/staa740](https://doi.org/10.1093/mnras/staa740)
- Messenger, C., & Veitch, J. 2013, *New J. Phys.*, 15, 053027, doi: [10.1088/1367-2630/15/5/053027](https://doi.org/10.1088/1367-2630/15/5/053027)
- Mohite, S. 2022, PhD thesis, University of Wisconsin-Milwaukee. <https://dc.uwm.edu/etd/2926/>
- Mould, M., Gerosa, D., Broekgaarden, F. S., & Steinle, N. 2022, *Mon. Not. Roy. Astron. Soc.*, 517, 2738, doi: [10.1093/mnras/stac2859](https://doi.org/10.1093/mnras/stac2859)
- Neijssel, C. J., Vigna-Gómez, A., Stevenson, S., et al. 2019, *Monthly Notices of the Royal Astronomical Society*, 490, 3740–3759, doi: [10.1093/mnras/stz2840](https://doi.org/10.1093/mnras/stz2840)
- Oriol, A.-P., Virgile, A., Colin, C., et al. 2023, *PeerJ Computer Science*, 9, e1516, doi: [10.7717/peerj-cs.1516](https://doi.org/10.7717/peerj-cs.1516)
- Pattabiraman, B., Umbreit, S., Liao, W.-k., et al. 2013, *The Astrophysical Journal Supplement Series*, 204, 15, doi: [10.1088/0067-0049/204/2/15](https://doi.org/10.1088/0067-0049/204/2/15)
- Payne, E., Kremer, K., & Zevin, M. 2024, *Astrophys. J. Lett.*, 966, L16, doi: [10.3847/2041-8213/ad3e82](https://doi.org/10.3847/2041-8213/ad3e82)
- Petrovich, C., & Antonini, F. 2017, *Astrophys. J.*, 846, 146, doi: [10.3847/1538-4357/aa8628](https://doi.org/10.3847/1538-4357/aa8628)
- Portegies Zwart, S. F., & McMillan, S. 2000, *Astrophys. J. Lett.*, 528, L17, doi: [10.1086/312422](https://doi.org/10.1086/312422)
- Portegies Zwart, S. F., & Yungelson, L. R. 1998, *Astron. Astrophys.*, 332, 173. <https://arxiv.org/abs/astro-ph/9710347>
- Qin, Y., Fragos, T., Meynet, G., et al. 2018, *Astron. Astrophys.*, 616, A28, doi: [10.1051/0004-6361/201832839](https://doi.org/10.1051/0004-6361/201832839)
- Ray, A., Hernandez, I. M., Mohite, S., Creighton, J., & Kapadia, S. J. 2023, *Phys. Rev. D*, 107, 083027, doi: [10.1103/PhysRevD.107.083027](https://doi.org/10.1103/PhysRevD.107.083027)
- Ray, A., & Kalogera, V. 2025. <https://arxiv.org/abs/2510.18867>
- Ray, A., Magaña Hernandez, I., Breivik, K., & Creighton, J. 2025, *Astrophys. J.*, 991, 17, doi: [10.3847/1538-4357/adf22a](https://doi.org/10.3847/1538-4357/adf22a)
- Rodriguez, C. L., Zevin, M., Amaro-Seoane, P., et al. 2019, *Phys. Rev. D*, 100, 043027, doi: [10.1103/PhysRevD.100.043027](https://doi.org/10.1103/PhysRevD.100.043027)
- Rodriguez, C. L., Zevin, M., Pankow, C., Kalogera, V., & Rasio, F. A. 2016, *Astrophys. J. Lett.*, 832, L2, doi: [10.3847/2041-8205/832/1/L2](https://doi.org/10.3847/2041-8205/832/1/L2)
- Rodriguez, C. L., Weatherford, N. C., Coughlin, S. C., et al. 2022, *The Astrophysical Journal Supplement Series*, 258, 22, doi: [10.3847/1538-4365/ac2edf](https://doi.org/10.3847/1538-4365/ac2edf)
- Romero-Shaw, I. M., Talbot, C., Biscoveanu, S., et al. 2020, *Monthly Notices of the Royal Astronomical Society*, 499, 3295, doi: [10.1093/mnras/staa2850](https://doi.org/10.1093/mnras/staa2850)
- Roy, S. K., van Son, L. A. C., & Farr, W. M. 2025, *Class. Quant. Grav.*, 42, 225008, doi: [10.1088/1361-6382/ae1921](https://doi.org/10.1088/1361-6382/ae1921)
- Sadiq, J., Dent, T., & Gieles, M. 2023, *The Astrophysical Journal*, 960, 65, doi: [10.3847/1538-4357/ad0ce6](https://doi.org/10.3847/1538-4357/ad0ce6)
- Sigurdsson, S., & Hernquist, L. 1993, *Nature*, 364, 423, doi: [10.1038/364423a0](https://doi.org/10.1038/364423a0)
- Speagle, J. S. 2020, *Monthly Notices of the Royal Astronomical Society*, 493, 3132, doi: [10.1093/mnras/staa278](https://doi.org/10.1093/mnras/staa278)
- Spera, M., & Mapelli, M. 2017, *Mon. Not. Roy. Astron. Soc.*, 470, 4739, doi: [10.1093/mnras/stx1576](https://doi.org/10.1093/mnras/stx1576)
- Stevenson, S., Sampson, M., Powell, J., et al. 2019, doi: [10.3847/1538-4357/ab3981](https://doi.org/10.3847/1538-4357/ab3981)
- Stevenson, S., Vigna-Gómez, A., Mandel, I., et al. 2017, *Nature Commun.*, 8, 14906, doi: [10.1038/ncomms14906](https://doi.org/10.1038/ncomms14906)
- Stone, N. C., Metzger, B. D., & Haiman, Z. 2017, *Mon. Not. Roy. Astron. Soc.*, 464, 946, doi: [10.1093/mnras/stw2260](https://doi.org/10.1093/mnras/stw2260)
- Talbot, C., & Golomb, J. 2023, *Mon. Not. Roy. Astron. Soc.*, 526, 3495, doi: [10.1093/mnras/stad2968](https://doi.org/10.1093/mnras/stad2968)
- Talbot, C., & Thrane, E. 2018, *Astrophys. J.*, 856, 173, doi: [10.3847/1538-4357/aab34c](https://doi.org/10.3847/1538-4357/aab34c)
- Tiwari, V., & Fairhurst, S. 2021, *Astrophys. J. Lett.*, 913, L19, doi: [10.3847/2041-8213/abfb67](https://doi.org/10.3847/2041-8213/abfb67)
- Tong, H., et al. 2025. <https://arxiv.org/abs/2509.04151>
- van Son, L. A. C., de Mink, S. E., Chruślińska, M., et al. 2023, *The Astrophysical Journal*, 948, 105, doi: [10.3847/1538-4357/acbf51](https://doi.org/10.3847/1538-4357/acbf51)
- van Son, L. A. C., de Mink, S. E., Renzo, M., et al. 2022a, *Astrophys. J.*, 940, 184, doi: [10.3847/1538-4357/ac9b0a](https://doi.org/10.3847/1538-4357/ac9b0a)
- van Son, L. A. C., de Mink, S. E., Callister, T., et al. 2022b, *Astrophys. J.*, 931, 17, doi: [10.3847/1538-4357/ac64a3](https://doi.org/10.3847/1538-4357/ac64a3)
- Vitale, S., Gerosa, D., Farr, W. M., & Taylor, S. R. 2020, *Springer*, 101, 124064, doi: https://doi.org/10.1007/978-981-16-4306-4_45
- Wang, Y.-Z., Li, Y.-J., Gao, S.-J., Tang, S.-P., & Fan, Y.-Z. 2025. <https://arxiv.org/abs/2510.22698>

- Wong, K. W. K., Breivik, K., Kremer, K., & Callister, T. 2021, Phys. Rev. D, 103, 083021, doi: [10.1103/PhysRevD.103.083021](https://doi.org/10.1103/PhysRevD.103.083021)
- Woosley, S. E. 2017, Astrophys. J., 836, 244, doi: [10.3847/1538-4357/836/2/244](https://doi.org/10.3847/1538-4357/836/2/244)
- Wysocki, D., Lange, J., & O’Shaughnessy, R. 2019, Physical Review D, 100, 043012, doi: [10.1103/PhysRevD.100.043012](https://doi.org/10.1103/PhysRevD.100.043012)
- Zevin, M. 2020, Constraining the Origins of Binary Black Holes using Multiple Formation Pathways, 1.0, Zenodo, doi: [10.5281/zenodo.4277620](https://doi.org/10.5281/zenodo.4277620)
- Zevin, M., & Bavera, S. S. 2022, Astrophys. J., 933, 86, doi: [10.3847/1538-4357/ac6f5d](https://doi.org/10.3847/1538-4357/ac6f5d)
- Ziegler, J., & Freese, K. 2021, Phys. Rev. D, 104, 043015, doi: [10.1103/PhysRevD.104.043015](https://doi.org/10.1103/PhysRevD.104.043015)
- Ziosi, B. M., Mapelli, M., Branchesi, M., & Tormen, G. 2014, Mon. Not. Roy. Astron. Soc., 441, 3703, doi: [10.1093/mnras/stu824](https://doi.org/10.1093/mnras/stu824)